Elaboration of PEG/PA66 blends in a twin-screw batch-type mini-extruder: Process study and modelling

Jonathan Leblanc, Fernand Pla, Mathilde Mercier, Pascal Pitiot

Chemical Engineering Science 64 (2009) 1918 – 1926

Contents lists available at ScienceDirect

Chemical Engineering Science

journal homepage: www.elsevier.com/locate/ces

Elaboration of PEG/PA66 blends in a twin-screw batch-type mini-extruder: Process study and modelling

Jonathan Leblanc[a], Fernand Pla[a,*], Mathilde Mercier[b], Pascal Pitiot[b]

[a]Laboratoire des Sciences du Génie Chimique, Nancy université, CNRS, 1 rue Grandville, BP 20451, F-54001 Nancy, France
[b]Rhodia Recherches & Technologies – CRTL, Groupe Polymères, 85 rue des Frères Perret, BP 62, F-69192 Saint-Fons Cedex, France

ARTICLE INFO

Article history:
Received 23 September 2008
Received in revised form 10 December 2008
Accepted 23 December 2008
Available online 22 January 2009

Keywords:
Polymers
Blends
Morphology
Particles size distribution
Mathematical modelling

ABSTRACT

This paper deals with the development of the morphology in polyethylene glycol (PEG) and polyamide 66 (PA66) immiscible blends exhibiting an extremely low viscosity ratio ($\eta_{PEG}/\eta_{PA66} = 3-4 \times 10^{-5}$). These materials were obtained by melt mixing, under different operating conditions, using a twin-screw batch-type DSM mini-extruder.

Scanning electron microscopy, followed by quantitative image analysis was used to determine PEG particles size distribution (PSD) as a function of blends composition and screw rotation speed. Experiments carried out with two mixing time (5 and 10 min) showed no significant difference of PSD. So, to avoid thermal degradation of the products, the mixing time was set up at 5 min for all experiments. The influence of PEG concentration and screw rotation speed on PSD appeared to be similar to that obtained in a previous study for the same blends elaborated in a Haake internal mixer. The results clearly showed that the average particle diameters decreased as screw rotation speed increased and as PEG concentration decreased. However, this decrease is less important using the twin-screw batch-type mini-extruder with which the particle sizes are smaller. The particles sizes were then correlated to blend composition, shear rate and viscosity ratio owing to an extension of Serpe's model. The unknown parameters of the corresponding model were estimated on the basis of experimental data. This enabled then to predict with a good precision the influence of the process operating conditions on the morphology of the dispersed phase.

1. Introduction

The manufacture of polymer blends is a convenient way to obtaining innovative materials. It is often cheaper and more flexible than conventional polymer synthesis. With immiscible polymers, the morphology of the dispersed phase is a critical key point in connection with the properties of the corresponding blends.

This morphology can be controlled by different process parameters and products properties, such as

(i) The type of mixer (Favis and Therrien, 1991; Thomas and et Groeninckx, 1999).
(ii) The mixing time (Favis, 1990; Thomas and et Groeninckx, 1999).
(iii) The shear rate (Favis, 1990; Ghodgaonkar and Sundararaj, 1998; Serpe et al., 1990; Sundararaj and Macosko, 1995; Thomas and et Groeninckx, 1999).
(iv) The blend composition (Favis and Chalifoux, 1988; Favis and Therrien, 1991; Serpe et al., 1990; Sundararaj and Macosko, 1995; Thomas and et Groeninckx, 1999)
(v) The viscosity ratio between the components (Favis and Chalifoux, 1987, 1988; Favis and Therrien, 1991; Serpe et al., 1990; Wu, 1987).
(vi) The interfacial tension (Wu, 1987) .

Taylor (1932, 1934)studied the deformation and breakup of Newtonian droplets in a simple shear field. By balancing shear and interfacial forces, he obtained a relationship able to predict the maximum drop diameter, d:

$$d = \frac{16\gamma(p+1)}{\dot{\gamma}\eta_m(19p+16)} \quad (1)$$

where, $\dot{\gamma}$ is the shear rate, p is the ratio of the viscosity of the dispersed phase (η_d) over that of the matrix (η_m) and γ is the interfacial tension.

However, this relation is valid for $p < 2.5$ and only for small deformations in a Newtonian media.

* Corresponding author. Tel.: +33 3 83 17 50 49; fax: +33 3 83 17 51 55.
E-mail address: fernand.pla@ensic.inpl-nancy.fr (F. Pla).

0009-2509/$ - see front matter © 2009 Elsevier Ltd. All rights reserved.
doi:10.1016/j.ces.2008.12.039

Taylor's work was completed by an interesting experimental study (Grace, 1982) on the breakup of Newtonian droplets in both simple and extensional shear flows. Grace showed that the breakup is possible for $p>4$ in a simple shear field and for any viscosity ratios in an extensional shear flow.

However, Taylor's theory is hardly applicable to viscoelastic systems, like polymer blends, for which elasticity has a strong effect on the dispersion mechanisms.

Wu (1987) studied then the drop break up in polymer blends and proposed the following empirical equation to predict the number average diameter of the dispersed phase, d_n:

$$\frac{\dot{\gamma}\eta_m d_n}{\gamma} = 4(p)^{\pm 0.84} \tag{2}$$

In this equation, the exponent is positive when p is higher than 1 and negative when p is lower than 1.

Nevertheless in this work, Wu did not consider the influence of the dispersed phase concentration, which is generally marked (Favis and Chalifoux, 1988; Favis and Therrien, 1991; Serpe et al., 1990; Sundararaj and Macosko, 1995, Thomas and et Groeninckx, 1999).

Serpe et al. (1990) introduced then the influence of the blend composition. They replaced the viscosity of the matrix by the viscosity of the blend (η_b) and introduced the following empirical function:

$$F(\varphi) = 1 - (4\varphi_d\varphi_m)^{0.8} \tag{3}$$

where φ_d and φ_m are the volume fractions of the dispersed phase and the matrix, respectively. Finally, they obtained the following power law relationship:

$$We^* = 4(\eta^*)^{\pm 0.84} \tag{4}$$

where

$$We^* = \frac{\dot{\gamma}\eta_b d_n F(\varphi)}{\gamma} \tag{5}$$

and

$$\eta^* = \left(\frac{\eta_d}{\eta_b}\right) \tag{6}$$

Most studies have been developed on binary systems exhibiting a viscosity ratio comprised between 0.01 and 20.

The present work concerns the manufacture of polyethylene glycol/polyamide 66 (PEG/PA66) blends exhibiting an extremely low viscosity ratio ($\eta_{PEG}/\eta_{PA66} = 3\text{–}4\times10^{-5}$) and elaborated using a twin-screw batch-type DSM mini-extruder.

It follows a previous study (Leblanc et al., 2007), where the same blends were elaborated using an internal Haake mixer in which the shear rates were lower than those developed with the mini-extruder.

Its main objective is the construction of a model able to predict the influence of the main process parameters and products properties on the resulting blends morphology.

2. Experimental part

2.1. Materials

2.1.1. Polymers

PA66 was provided by Rhodia, while PEG was purchased from Sigma Aldrich. The main properties of these polymers are summarized in Table 1.

2.1.2. Solvents

2,2,2—Trifluoroethanol (TFE), chloroform-D ($CDCl_3$) and dichloromethane (CH_2Cl_2) were purchased from Sigma Aldrich.

Table 1
Main properties of PA66 and PEG.

	Density[a] ($g\,cm^{-3}$)	Melting point[b] (°C)	Mn[b] ($g\,mol^{-1}$)
Polyamide 66	1.145	265	–
Polyethylene glycol	1.215	55–58	2.000

[a]Measured at ambient temperature using a helium displacement pycnometer.
[b]Number average molar mass obtained from suppliers.

Table 2
Operating conditions used for the elaboration of the blends in the mini-extruder.

Runs*	Screw rotation speed (rpm)	PEG/PA (%)	Mixing time (min.)	Quench
MC-1	100	10/90	5	Liquid nitrogen
MC-2	100	20/80	5	Liquid nitrogen
MC-3	100	30/70	5	Liquid nitrogen
MC-4	175	10/90	5	Liquid nitrogen
MC-5	175	20/80	5	Liquid nitrogen
MC-6	175	30/70	5	Liquid nitrogen
MC-7	175	20/80	5	Liquid nitrogen
MC-8	175	20/80	10	Liquid nitrogen
MC-9	175	20/80	5	Water

*Operating temperature: 275 °C.

2.2. Blends elaboration

Blends were prepared in a 15 mL corotative twin-screw batch-type mini-extruder developed by DSM-Research. The two polymers were introduced simultaneously, under nitrogen atmosphere. After 5 min of mixing at 275 °C, a blend sample was removed and quenched in liquid nitrogen.

Operating conditions of all runs are reported in Table 2. Two rotors speeds were used (100 and 175 rpm). The feeding PEG weight fractions were between 10% and 30%. Seven runs were carried out according to the protocol described above. Run MC-7 corresponds to the duplication of run MC-5.

Complementary runs were also performed in order to evaluate the influence of the mixing time (run MC-8) and the quench type (run MC-9).

2.3. Analytical techniques

2.3.1. Viscosity

The viscosity of PEG was measured using a dynamic stress rheometer (Rheometrics Scientific—SR 200—with parallel plate geometry 40 mm diameter). It showed a Newtonian behavior with a viscosity of 4×10^{-3} Pa s at 275 °C. The viscosity of PA was 145, 105.6 and 75.2 Pa s for 1000, 2500 and 5000 s^{-1}, respectively (data from suppliers).

2.3.2. Density

Densities of PEG and PA66 were measured at ambient temperature using a helium displacement pycnometer (ACCUPYC 1330).

2.3.3. Morphology analysis

Blends morphology was examined using a JEOL JSM-T330A scanning electron microscope (SEM).

Before observations, the samples were held in liquid nitrogen, cryofractured and immersed in boiling dichloromethane overnight to remove the dispersed phase (PEG). They were then dried and their surface was coated with gold to make them conductive.

The images obtained with the MEB provide a qualitative description of the microstructure of the blends. The analysis of these images allows then a quantification of the morphology.

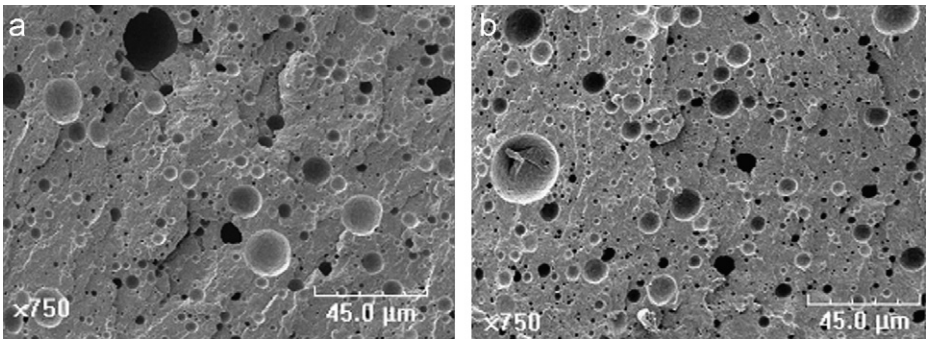

Fig. 1. SEM micrographs of blends resulting from runs carried out under identical operating conditions: (a) =run MC-5 and (b) =run MC-7.

The MEB gives digital images with 256 levels of gray. The intersection of the cross section and the various dispersed particles reveals objects which can be extracted from the image. For that, a first stage consists (i) in working over again the image in order to improve the contrast of certain particles compared to the bottom of the image, (ii) to remove certain isolated points and (iii) to separate certain objects which are connected. This work is carried out using the software PAINT SHOP PRO which allows making the final improvement of the images.

The images are then binarized by a threshold which consists in assigning the value 1 to each pixel having a level of gray equal to or higher than a certain threshold. This operation makes it possible to allot to the objects which will be analyzed, the value of 1 while the bottom of the image will receive the value of 0. This work is realized by use of a software of image processing, IMAGE TOOL 3.0.

Once these operations carried out, the objects of the image can be counted. Various morphological parameters, among which the surface of the objects, can be automatically measured. From the values of the surfaces, the diameter of each particle is then calculated by means of the following formula:

$$d_i = \left(\frac{4A_i}{\pi}\right)^{1/2} \tag{7}$$

where d_i is the diameter of the particle and A_i is the surface of the object measured on the image

It is however important to recall that the particles are three-dimensional and that they can thus be cut at various levels. In this work, this aspect was neglected: no correction was brought on the values of the diameters, which thus correspond to the diameters of the sections observed. This finally amounts considering that all the particles are cut on the level of their equatorial plan.

A distribution of these diameters can then be obtained by distributing the various objects in groups of diameters. The limits of intervals of these groups are founded on a linear scale of these diameters.

When the distribution is too broad so that all the particles can be observed under only one magnification, the analysis is performed at two different magnifications: the first allows taking into account the small particles whereas the second allows quantifying the largest. The total distribution is then obtained by combining the two distributions. For that, each distribution is normalized by the surface of the images to which the analysis is related.

The number average diameters, d_n, were then calculated using the following equation:

$$d_n = \frac{\sum N_i d_i}{\sum N_i} \tag{8}$$

where N_i is the number of particles.

Table 3
Parameters useful for the mathematical model development.

Runs	d_n (µm)	ϕ_d	$\dot{\gamma}$ (s^{-1})	η_m (Pa s)	η_b (Pa s)	We^*	η^* ($\times 10^{-5}$)
MC-1	1.57	0.049	1570	124.1	74.7	42.51	5.5
MC-2	1.78	0.142	1570	124.1	28.8	11.02	14.2
MC-3	1.78	0.205	1570	124.1	14.9	3.78	27.4
MC-4	1.48	0.071	2747.5	100.9	49.2	41	8.3
MC-5	1.52	0.154	2747.5	100.9	21.2	11.25	19.3
MC-6	1.61	0.218	2747.5	100.9	11.2	4.08	36.7
MC-7	1.51	0.162	2747.5	100.9	19.4	9.77	21.0
MC-8	1.50						
MC-9	1.53						

2.3.4. Blends composition

The actual concentration of PEG in blends was measured by 1H NMR spectroscopy. A sample was dissolved in a mixture of TFE/$CDCl_3$ (50/50). Measurements were performed on a Brucker 300 MHz (model Avance 300) spectrometer. The relative proportion of PEG was established by integrating specific peaks of the two polymers. The peaks at 3.65–3.3 ppm correspond to PEG hydrogen atoms while those at 1.78–1.25 ppm correspond to polyamide hydrogen atoms. Integral value of TFE satellites (at 4.12–3.96 ppm) were subtracted from that corresponding to PEG.

3. Results and discussion

3.1. Experimental study of the process

The values of number average diameters d_n of each blend, summarized in Table 3, allow making the following first comments.

3.1.1. Experimental reproducibility

Fig. 1 gives SEM micrographs of blends resulting from runs MC-5 and MC-7 carried out under the same operating conditions. It shows the good experimental reproducibility of the technique used to elaborating the materials.

This is clearly confirmed by the similar particle size distribution (PSD) reported in Fig. 2 and the corresponding average diameters, $d_n = 1.52$ and 1.51 µm, respectively (Table 3).

3.1.2. Influence of mixing time

Fig. 3 illustrates the influence of the mixing time on the PSD. A change of this time from 5 to 10 min (runs MC-5 and MC-8) causes only a very small decrease in the average diameter d_n (1.3%).

Moreover, Fig. 4 clearly shows that the corresponding PSD of these two blends are quite identical. Therefore,to avoid thermal degradations of the products during their elaboration, the mixing time then used for all other runs was 5 min.

3.1.3. Influence of PEG concentration

Fig. 5 illustrates the influence of the blends composition on their morphology. It appears that the dispersed phase size increases as the PEG concentration increases.

However, examination of the corresponding average diameters (Fig. 6) shows that this tendency stays limited and is less important than the one observed in blends obtained by the use of Haake internal mixer (Leblanc et al., 2007).

As for the blends elaborated using Haake internal mixer, this limited increase can be due to the high viscosity of the matrix, which impedes the agglomeration of the dispersed phase and decreases the coalescence rate.

3.1.4. Influence of the screw rotation speed

Fig. 7 shows that the PEG particles sizes seem to decrease as the screw rotation speed is increased.

However, examination of the corresponding average diameters (Fig. 8) shows that, using the mini-extruder, these diameters are smaller than those obtained with Haake internal mixer. This is probably due to the higher shear rates ($\dot{\gamma}$) developed in the extruder: 1570 and 2747.5 s^{-1} (Table 3), against 39.6, 59.4 and 79.1 s^{-1} developed in Haake internal mixer (Leblanc et al., 2007). Moreover, with the extruder the diameters are already very small for a screw rotation speed of 100 rpm (i.e. a shear rate of 1570 s^{-1}), with, as shown in Fig. 8, a very slight decrease as the screw rotation speed is increased from 100 to 175 rpm (i.e. as the shear rate is increased from 1570 to 2747.5 s^{-1}).

As shown in Fig. 8, with Haake internal mixer, these diameters are larger than with the extruder and this is in favor of a more pronounced decrease of the particle diameters as the Haake rotors rotation speed is increased from 100 to 200 rpm (i.e. as the shear rate is increased from 39.6 to 79.1 s^{-1}).

3.1.5. Influence of the quench

SEM micrographs (Fig. 9) show that the two blends elaborated under the same processing conditions (MC-5 and MC-9) but with a difference in the liquid used for the quenching step are quite similar.

This is confirmed by the corresponding PSD (Fig. 10).

3.1.6. Modelling of the process: Influence of the process parameters and products properties on the blends morphology

As in our previous paper (Leblanc et al., 2007) the influence of the process parameters and products main characteristics was at first studied through the establishment of the corresponding power law linking the modified Weber number, to the viscosity ratio between the two polymers, η^* i.e.:

$$We^* = \theta_0(\eta^*)^{\theta_1} \tag{9}$$

where θ_0 and θ_1 are coefficients of the model.

We^* and η^* were determined for each experiment through the calculation of:

- The volume fractions, ϕ_d and ϕ_m, of the two components, determined thanks to the PEG weight percentage (measured by 1H NMR) and density (measured at ambient temperature).

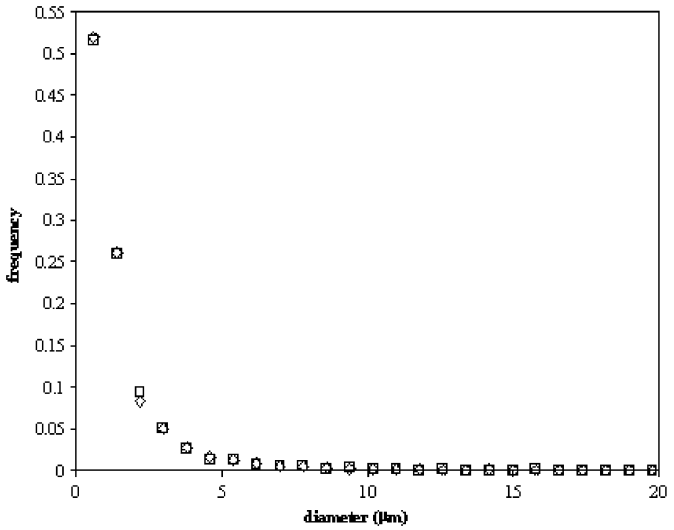

Fig. 2. Particles size distribution of blends resulting from runs carried out under identical operating conditions: (◇) = run MC-5 and (□) = run MC-7.

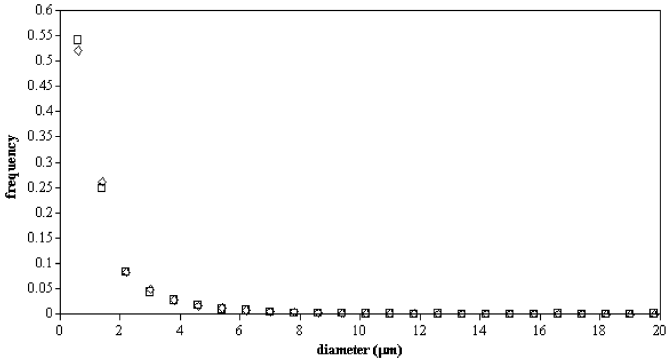

Fig. 4. Particles size distribution of blends obtained with different mixing times (◇) = 5 min and (□) = 10 min.

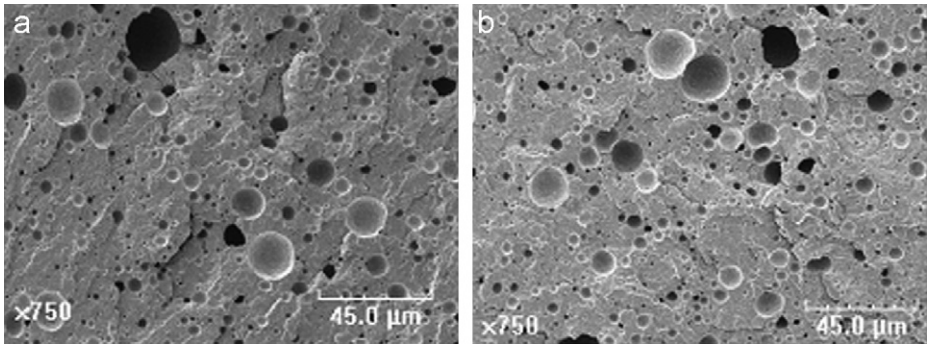

Fig. 3. SEM micrographs of blends obtained with different mixing times: (a) =5 min and (b) =10 min.

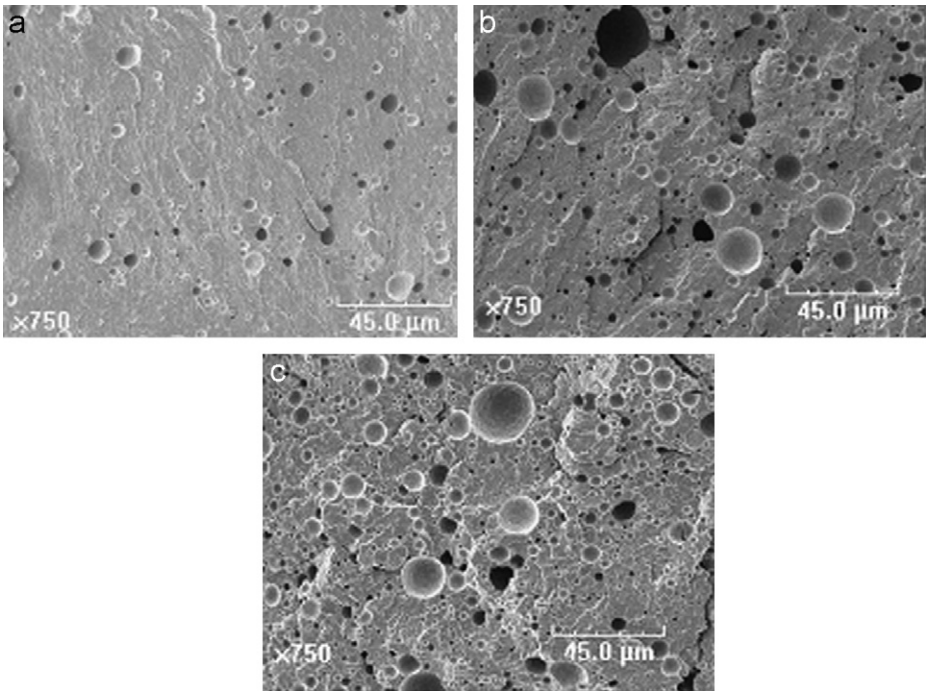

Fig. 5. SEM micrographs of blends obtained with the same screw rotation speed (175 rpm) and different PEG concentrations: (a) =10% wt, (b) =20% wt and (c) =30% wt.

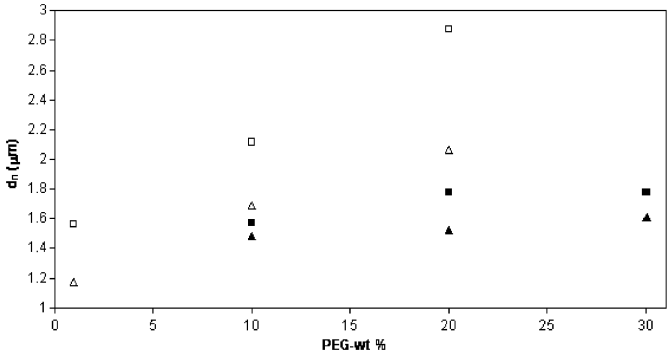

Fig. 6. Effect of PEG concentration on the number average particle diameter of blends obtained with different screw rotation speeds using the mini-extruder ((■)=100 rpm and (▲) = 175 rpm) and different rotors rotation speeds using the Haake internal mixer ((□) = 100 rpm and (△) = 200 rpm).

- The shear rate in the mini-extruder, determined by use of the following empirical equation, established by Rhodia (unpublished results):

$$\dot{\gamma} = 15.7N \tag{10}$$

where $\dot{\gamma}$ and N are the shear rate (s^{-1}) and the screw rotation speed (rpm), respectively.

- The matrix viscosity, η_m, estimated at a given shear rate by assuming a power law behavior between each of the values reported for 1000, 2500 and 5000 s^{-1},
- The blends viscosity, η_b, estimated through the log-linear mixing rule generally recommended for polymer blends when the viscosities of the components are very different (Grizzuti et al., 2000)

$$\log(\eta_b) = \phi_d \log(\eta_d) + \phi_m \log(\eta_m) \tag{11}$$

- The interfacial tension at 275 °C, obtained using the following harmonic average equation:

$$\gamma = \gamma_1 + \gamma_2 - 4\frac{\gamma_{1p}\gamma_{2p}}{\gamma_{1p} + \gamma_{2p}} - 4\frac{\gamma_{1d}\gamma_{2d}}{\gamma_{1d} + \gamma_{2d}} \tag{12}$$

where γ is the interfacial tension between polymers 1 and 2, γ_i ($i = 1$ and 2) is the surface tension of polymer i, γ_{ip} and γ_{id} are the polar and the dispersive fractions of the surface tension of polymer i, respectively.

The surface tensions of PEG and PA66 together with their polar and dispersive contributions were determined at 275 °C, using values issued from the literature for other temperatures and from their corresponding temperature coefficient ($d\gamma_i/dT$) and polarity ($x^{ip}=\gamma_{ip}/\gamma_i$) (Wu, 1989).

Finally, according to Eq. (11), the resulting interfacial tension between PA and PEG at 275 °C is 3.2 mN/m.

Table 3 reports the values of φ_d, $\dot{\gamma}$, η_m, η_b, We^* and η^*, corresponding to each experiment.

3.1.7. Estimation of the model parameters

The parameters θ_0 and θ_1, of the power law (Eq. (8)) were determined using a multi-linear regression (Nobelen et al., 2006).

Runs MC-2, MC-4 and MC-6 were used for this purpose while runs MC-1 and MC-3 were then used for the model validation.

Table 4 presents the estimated value found for each parameter together with the corresponding reduced confidence intervals with a risk of 10%.

The number of degrees of freedom, v_I, for the identification experiments, is given by the difference between the number of runs and the number of the coefficients of the model. Thus, v_i, =1 (3 runs minus 2 model coefficients).

The variance, σ_i^2, was obtained by dividing the sum of squared deviations between the experimental and the model values of $\ln(We_i^*)$ by v_I. Its value is σ_i^2 is 0.150.

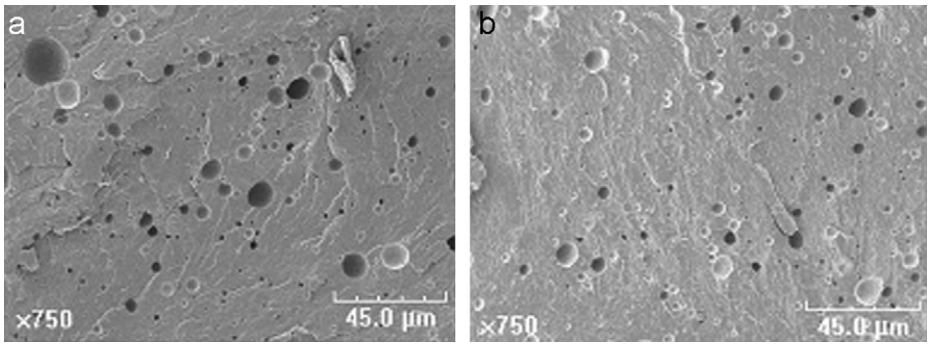

Fig. 7. SEM micrographs of blends obtained with different screw rotation speeds [(a) =100 rpm and (b) =175 rpm] and the same PEG concentration (10% wt).

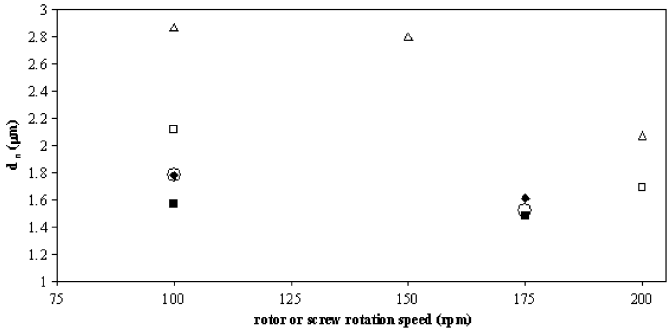

Fig. 8. Effects of the mini-extruder and Haake internal mixer rotation speeds on the average particles diameter of blends with different PEG concentrations. Mini-extruder ((■)=10% wt, (○)=20% wt and (♦)=30% wt); Haake internal mixer: ((□)=10% wt and (△) = 20% wt).

Confidence intervals were used to define if the values of the parameters are significantly different from zero. It is well established that the uncertainty on the estimated parameters is all the more important if the interval is centred on zero. In the present case, it is clear that none of the parameters needed to be rejected.

3.1.8. Validation of the model

The concordance between simulated and experimental values of $ln(We_i^*)$ is shown in Fig. 11. A 10% confidence interval was established as

$$\hat{y} - \mathrm{Stu}_{0.95}\sqrt{(\sigma_m^2)} \leqslant y \leqslant \hat{y} + \mathrm{Stu}_{0.95}\sqrt{(\sigma_m^2)} \tag{13}$$

where $\hat{y}$ and y are the simulated and the experimental values, respectively, $\mathrm{Stu}_{0.95}$ is the Student criterion with a risk of 5% and σ_m^2 is the experimental variance.

The full lines represent the confidence interval for the measurement. It appears that all experiments are within this confidence interval, which indicates an apparent acceptable fitting of the data measured.

Fischer–Snedecor's test was also applied to the present model. The validation of the model with a risk of 10% implies the verification of the following relationship:

$$\frac{1}{F_{0.05}(\upsilon_j, \upsilon_i)} \leqslant \frac{\sigma_i^2}{\sigma_j^2} \leqslant F_{0.05}(\upsilon_i, \upsilon_j) \tag{14}$$

where σ_k^2 is the error variance and $F_{0.05}(\upsilon_i, \upsilon_j)$ is Fischer–Snedecor's value with a probability of 5% and with the degrees of freedom υ_i and υ_j. The corresponding results are presented in Table 5.

For the validation experiments, the number of degrees of freedom, v_v, is 2 (2 runs). The validation variance, σ_v^2, obtained by dividing the sum of square deviations between simulated and experimental values of $ln(We_i^*)$ by v_v, is equal to 0.156.

For duplication experiments, since the mean value of $\ln(We_i^*)$ was used to calculate the sum of squares, the number of degrees of freedom, v_r, is 1 (2 runs minus 1 mean value). The duplication variance, σ_r^2 was obtained by dividing the sum of square deviations between experimental data and the mean value of $ln(We_i^*)$, by v_r. So $\sigma_r^2 = 0.0108$.

This shows that the ratios of the variances respect Fischer-Snedecor's condition, which also proves the acceptable quality of the model.

Finally, the model resulting from this first approach is:

$$We^* = 2.6 \times 10^{-5}(\eta^*)^{-1.5} \tag{15}$$

This shows that the value of the power index parameter is close to that of the model previously obtained for the process using the internal mixer (Leblanc et al., 2007) i.e.:

$$We^* = 1.1 \times 10^{-6}(\eta^*)^{-1.44} \tag{16}$$

The main difference between these two models is the value of the parameter θ_0.

3.1.9. Application of the model: error on the prediction

Fig. 12 shows the evolution of simulated and experimental values of We^* versus η^*. Dotted line is issued from the model while the two full lines correspond to the confidence interval of 10% (See Appendix A).

Although the model was validated, Fig. 12 clearly shows that its use to simulate carefully the results is not entirely satisfactory: the confidence interval on the results is still too large to enable an accurate prediction. So, a new model was developed to improve this prediction.

3.2. Improvement of the model

3.2.1. Proposed structure

According to these results and comments, an extension of this model was applied to these results. This extension consisted in:

- considering that the average diameter is not exactly an inverse function of the shear rate,
- replacing Eq. (9) by the following :

$$We^* = \theta_0(\eta^*)^{\theta_1}(\dot{\gamma})^{\theta_2} \tag{17}$$

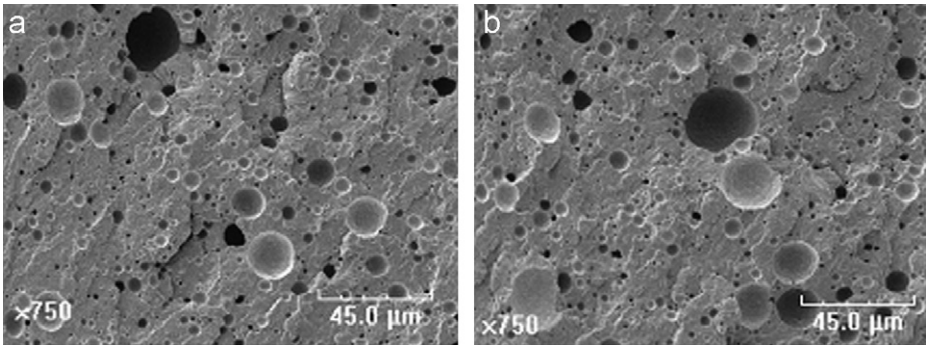

Fig. 9. SEM micrographs of blends resulting from runs carried under identical operating conditions except for the quenching recovery: (a) = run MC-5 with quench in liquid nitrogen and (b) =run MC-9 with quench in cold water.

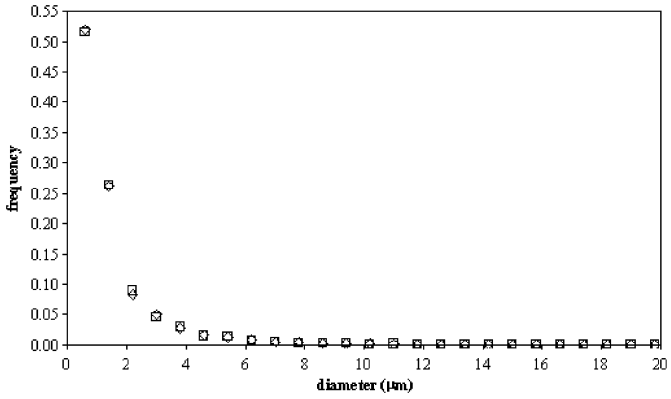

Fig. 10. Particles size distribution of blends resulting from runs carried out under identical operating conditions except for the quench recovery: (a) =run MC-5 with quench in liquid nitrogen and (b) =run MC-9 with quench in cold water.

Table 4
Values of the model parameters and corresponding reduced confidence intervals with a risk of 10%.

Model parameter	Estimated value	$\hat{\theta}^{red}_{min}$	$\hat{\theta}^{red}_{max}$
$ln\theta_0$	−10.55	−14.39	−13.35
θ_1	−1.50	−1.50	−1.39

Using Eq. (5), this led to the following equation:

$$\ln[\eta_b d_n F(\varphi)/\gamma] = \ln\theta_0 + \theta_1 \ln(\eta^*) + (\theta_2 - 1)\ln(\dot{\gamma}) + \varepsilon \quad (18)$$

where θ_0, θ_1 and θ_2 are the coefficients of the model and ε is the unknown corresponding experimental error.

To keep Serpe's formalism, the proposed model was then

$$\ln(We^*) = \ln\theta_0 + \theta_1 \ln(\eta^*) + \theta_2 \ln(\dot{\gamma}) + \varepsilon \quad (19)$$

3.2.2. Estimation of the new parameters

Four experiments (runs MC-2, MC-4, MC-5 and MC-6) were used to identify the model parameters.

Table 6 presents the estimated value of each new parameter, and the corresponding reduced confidence interval with a risk of 10%. This confidence interval was determined by using the identification variance, σ_1^2.

In this case, the number of degrees of freedom for the identification experiments, v_I, is equal to 1 (4 runs less 3 model coefficients) and the variance, σ_I^2, is 0.0001.

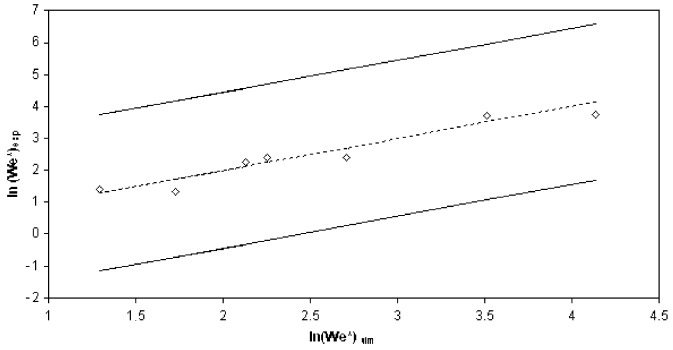

Fig. 11. Comparison of experimental and first simulated values of ln (We^*).

Table 5
Fischer–Snedecor's test applied to the model.

Variance ratio	$\frac{\sigma_i^2}{\sigma_j^2}$	(v_i, v_j)	$\frac{1}{F_{0.05}(v_j, v_i)}$	$F_{0.05}(v_i, v_j)$
Identification/duplication	15.08	1;1	0.006	161
Validation/identification	1.04	2;1	0.005	199.50
Validation/duplication	15.75	2;1	0.005	199.50

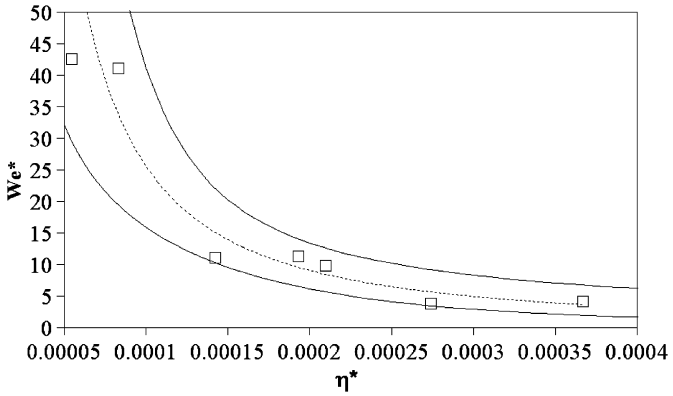

Fig. 12. Evolution of We^* versus η^* (dotted lines correspond to the model and full lines correspond to a confidence interval of 10%).

Table 6 shows that none of the coefficients needed to be rejected.

3.2.3. Validation of the model

Fig. 13 clearly shows the very good agreement between the simulated and experimental values of $\ln(We_i^*)$. The full lines represent

Table 6
New values of the model parameters and corresponding reduced confidence intervals with a risk of 10%.

Coefficient	Estimated value	$\hat{\theta}^{red}_{min}$	$\hat{\theta}^{red}_{max}$
$\ln\theta_0$	−17.74	−17.81	−17.66
θ_1	0.87	0.86	0.88
θ_2	−1.55	−1.56	−1.55

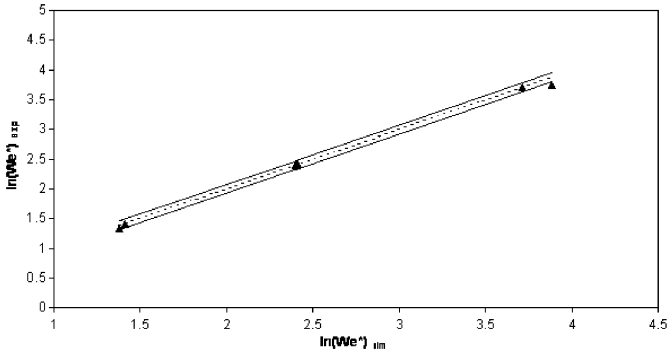

Fig. 13. Comparison of experimental and actual simulated values of ln (We^*).

Table 7
Fischer–Snedecor's test applied to the new model.

Variance ratio	$\frac{\sigma_i^2}{\sigma_j^2}$	(v_i, v_j)	$\frac{1}{F_{0.05}(v_j, v_i)}$	$F_{0.05}(v_i, v_j)$
Validation/identification	74.7	2;1	0.005	199.50

the confidence interval of 10% for the measurements. Almost all experiments (except one near the confidence interval) are within the confidence interval, which shows the good fitting of the measured data.

Two experiments (runs MC-1 and MC-3) were used for the validation of the model. For these experiments, the number of degrees of freedom, v_v, is 2 (2 runs). The validation variance, σ_v^2, is equal to 0.01.

The results of the Fischer–Snedecor's test are presented in Table 7. The ratios of the variances respect Fischer–Snedecor's condition, which proved the good quality of the model.

Finally, the model proposed for this process is

$$We^* = 1.98 \times 10^{-8}(\dot{\gamma})^{0.87}(\eta^*)^{-1.55} \quad (20)$$

It shows that PEG concentration, shear rate and the viscosity ratio between the two components are the key parameters of the process.

The model takes also into account the interfacial tension between PEG and PA66 which is used in the calculation of the modified Weber number.

Concerning the other parameters mentioned in the introduction of this paper, this work clearly shows the influence of the type of mixer which compares the Haake internal mixer and the batch-type mini-extruder and attributes this result to the different shear rates developed in these two instruments.

Moreover, if the effect of the mixing time was not intensively studied, the experimental results showed that for a mixing time up to 5 min the PSD of the resulting blends is not changed.

3.2.4. Model application: error on the prediction

Figs. 14 and 15 compare the evolution of the experimental and simulated values of We^* versus η^* for two different screw rotation speeds (100 and 175 rpm, respectively).

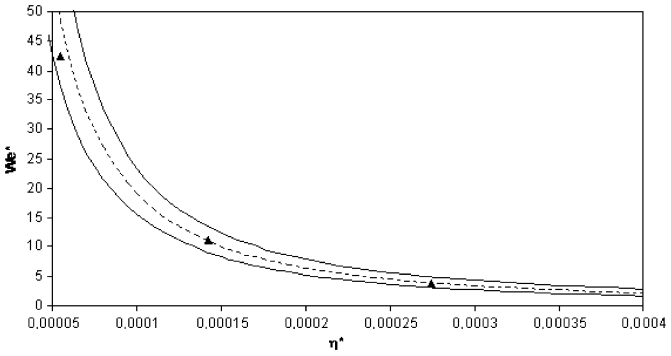

Fig. 14. Evolution of We^* versus η^* for a screw rotation speed of 100 rpm (dotted line correspond to a model and full lines correspond to a confidence interval of 10%).

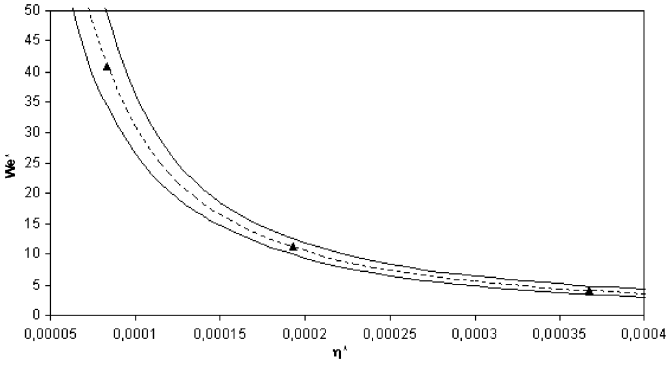

Fig. 15. Evolution of We^* versus η^* for a screw rotation speed of 175 rpm (dotted lines correspond to the model; full lines correspond to a confidence interval of 10%).

It is clear that with the new model, the confidence intervals are more narrowed which enables a more accurate prediction.

4. Conclusion

In this study, the morphology of PEG/PA66 blends, elaborated in a twin-screw batch-type mini-extruder, has been investigated. These two polymers present an extremely low viscosity ratio. The results allowed the following concluding remarks:

1. The influence of the main processing parameters on the dispersed phase size showed trends similar to others already observed, in a previous study, for the same blends elaborated using a Haake internal mixer.
2. PEG concentration, shear rate and viscosity ratio clearly appeared to be the main key parameters of the process. They were correlated to the observed dispersed phase size through a power law relationship between the modified Weber number and the viscosity ratio. The power law coefficient is very close to the one found for similar blends using the Haake internal mixer but differs from those established for systems with classical viscosity ratios [0.01–20].
3. However, although this model was validated, a more detailed analysis clearly showed that the confidence interval on the results was still too large to enable a sufficient accurate prediction.
4. This then led to modify this model considering that the average particles diameter is not exactly an inverse function of the shear rate. The resulting model enabled then to predict with a good precision the influence of the process operating conditions on the morphology of the dispersed phase.

Appendix A.

Let **Y** be the vector of the experimental responses, θ the vector of the model coefficients and ε the vector of the experimental errors. The model matrix, **X**, is obtained from the experiments realized and the model chosen.

The model is represented in the following matrix form:

$$\mathbf{Y} = \mathbf{X}\boldsymbol{\theta} + \varepsilon \tag{21}$$

If one considers an experiment, the difference between the calculated value $\hat{y}$ and the real value y is given by

$$(\hat{y} - y) = \mathbf{x}^t(\hat{\boldsymbol{\theta}} - \boldsymbol{\theta}) \tag{22}$$

where $\mathbf{x}^t$ is obtained from the experiment realized and the model chosen and $\hat{\theta}$ is the vector of the estimated coefficient value

The sum of squares of the difference between the calculated and real values of y is given by

$$(\hat{y} - y)^2 = \mathbf{x}^t(\hat{\boldsymbol{\theta}} - \boldsymbol{\theta})(\hat{\boldsymbol{\theta}} - \boldsymbol{\theta})^t\mathbf{x} \tag{23}$$

Yet, the variance of y, $V(y)$, can be calculated through:

$$V(y) = E[(\hat{y} - y)^2] = \mathbf{x}^t E[(\hat{\boldsymbol{\theta}} - \boldsymbol{\theta})(\hat{\boldsymbol{\theta}} - \boldsymbol{\theta})^t]\mathbf{x} \tag{24}$$

By definition, $E[(\hat{\boldsymbol{\theta}} - \boldsymbol{\theta})(\hat{\boldsymbol{\theta}} - \boldsymbol{\theta})^t$ is equal to the variance–covariance matrix, $\mathbf{V}(\hat{\boldsymbol{\theta}})$, given by

$$\mathbf{V}(\hat{\boldsymbol{\theta}}) = \mathbf{x}^t\sigma_m^2(\mathbf{X}^t\mathbf{X})^{-1}\mathbf{x} = E[(\hat{\boldsymbol{\theta}} - \boldsymbol{\theta})(\hat{\boldsymbol{\theta}} - \boldsymbol{\theta})^t] \tag{25}$$

with σ_m^2 the experimental variance

When the model is used for a prediction, the 10% confidence interval of the real value is given by

$$\hat{y} - \mathrm{Stu}_{0.95}\sqrt{V(y)} \leqslant y \leqslant \hat{y} + \mathrm{Stu}_{0.95}\sqrt{V(y)} \tag{26}$$

With Eqs. (13) and (14), the confidence interval can be written as

$$\hat{y} - \mathrm{Stu}_{0.95}\sqrt{(\sigma_m^2\mathbf{x}^t(\mathbf{X}^t\mathbf{X})^{-1}\mathbf{x})} \leqslant y \leqslant \hat{y} + \mathrm{Stu}_{0.95}\sqrt{(\sigma_m^2\mathbf{x}^t(\mathbf{X}^t\mathbf{X})^{-1}\mathbf{x})} \tag{27}$$

References

Favis, B.D., Chalifoux, J.P., 1987. The effect of viscosity ratio on the morphology of polypropylene/polycarbonate blends during processing. Polymer Engineering and Science 27, 1591–1600.

Favis, B.D., Chalifoux, J.P., 1988. Influence of composition on the morphology of polypropylene/polycarbonate blends. Polymer 29, 1761–1767.

Favis, B.D., 1990. The effect of processing parameters on the morphology of an immiscible binary blend. Journal of Applied Polymer Science 39, 285–300.

Favis, B.D., Therrien, D., 1991. Factors influencing structure formation and phase size in an immiscible polymer blend of polycarbonate and polypropylene prepared by twin screw extrusion. Polymer 32, 1474–1481.

Ghodgaonkar, P.G., Sundararaj, U., 1998. Prediction of dispersed phase drop diameter in polymer blends : the effect of elasticity. Polymer Engineering and Science 36, 1656–1665.

Grace, H.P., 1982. Dispersion phenomena in high viscosity immiscible fluid systems and application of static mixers as dispersion devices in such systems. Chemical Engineering Communications 14, 225–277.

Grizzuti, N., Giovanna, B., Iorio, G., 2000. Viscous behavior and mixing rules for immiscible model polymer blend. The Society of Rheology 44, 149–164.

Leblanc, J., Mercier, M., Fonteix, C., Pla, F., 2007. Design of blends with an extremely low viscosity ratio between the dispersed and continuous phases. Dependence of the dispersed phase size on the processing parameters. Macromolecular Symposia 259, 85–93.

Nobelen, M., Hoppe, S., Fonteix, C., Pla, F., Dupire, M., Jacques, B., 2006. Modeling of the rheological behaviour of polyethylene/supercritical CO_2 solutions. Chemical Engineering Science 61, 5334–5345.

Serpe, G., Jarrin, J., Dawans, F., 1990. Morphology-processing relationships in polyethylene–polyamide blends. Polymer Engineering and Science 30, 553–565.

Sundararaj, U., Macosko, C.W., 1995. Drop breakup and coalescence in polymer blends: the effects of concentration and compatibilisation. Macromolecules 28, 2647–2657.

Taylor, G.I., 1932. The viscosity of a fluid containing small drops of another fluid. Proceedings of the Royal Society of London A 138, 41–48.

Taylor, G.I., 1934. The formation of emulsions in definable fields of flow. Proceedings of the Royal Society of London A 146, 501–523.

Thomas, S., et Groeninckx, G.S., 1999. Reactive compatibilization of heterogeneous ethylene propylene rubber (EPM)/nylon 6 blends by the addition of compatibilizer precursor EPM-g-MA. Polymer 40, 5799–5819.

Wu, S., 1987. Formation of dispersed phase in incompatible polymer blends: interfacial and rheological effects. Polymer Engineering and Science 27, 335–343.

Wu, S., 1989. In: Brandup, J., Immergut, E.H. (Eds.), Polymer Handbook, 3rd ed. Wiley, New York, p. VI/411ff.